Figure Captions

Figure 1: A schematic illustration of the change in emission level (Z_e) associated with an increase in surface temperature (T_s) due to a doubling of CO_2 assuming a fixed atmospheric lapse rate. Note that the effective emission temperature (T_e) remains unchanged.

Figure 2: The annual-mean observed distribution of the clear-sky greenhouse effect G_{clear} (top), vertically-integrated water vapor concentration (middle), and sea surface temperature (bottom). Data are missing over land and ice-covered oceans due to uncertainties in their surface emission.

Figure 3: A time series of the tropical-mean interannual anomalies in clear-sky greenhouse trapping (G_{clear}) for 1985-1988 from ERBE observations (dashed line) and GFDL model simulations (dotted line). For reference, the tropical-mean anomalies in sea surface temperature are also shown (thick line).

Figure 4: The change in surface temperature (ΔT_s) for doubled CO_2 as a function of the water vapor feedback parameter (β_{H2O}). Results are shown for two different scenarios of other temperature dependent feedbacks (β_{other}) that encompass the current range of predictions in ΔT_s=1.5-4.5 K when β_{H2O}=0.4.

Figure 5: The upper tropospheric relative humidity (color) and cloud cover (grey) as observed from the Geostationary Operational Environmental Satellite (GOES-8) on April 27, 1999.

Figure 6: Height-latitude cross sections of the zonal-mean relative humidity for the month of July 1987 as produced by the European Centre for Medium-range Weather Forecasts (ECMWF) analysis system (left) and predicted by the GFDL General Circulation Model (GCM) (right).

Figure 7: The geographic distribution of relative humidity, vertically-averaged over the free troposphere for July 1987 from the ECMWF analyses (left) and the GFDL GCM (right).

Figure 8: A height-latitude schematic of the large-scale atmospheric trajectories involved in the transport and mixing of moisture within the troposphere.

Figure 9: Height-latitude cross-sections of the sensitivity of the outgoing longwave radiation to perturbations in water vapor Q_e (top) and temperature Q_T (bottom) in 100 hPa thick layers. The results are expressed in units of $Wm^{-2}K^{-1}$.

Figure 10: Distribution of cloud water (light blue) and precipitation (dark blue) simulated by the GFDL resolved cloud model. Note the difference in scale between the regions of active convection with respect to a typical GCM grid box (yellow box).

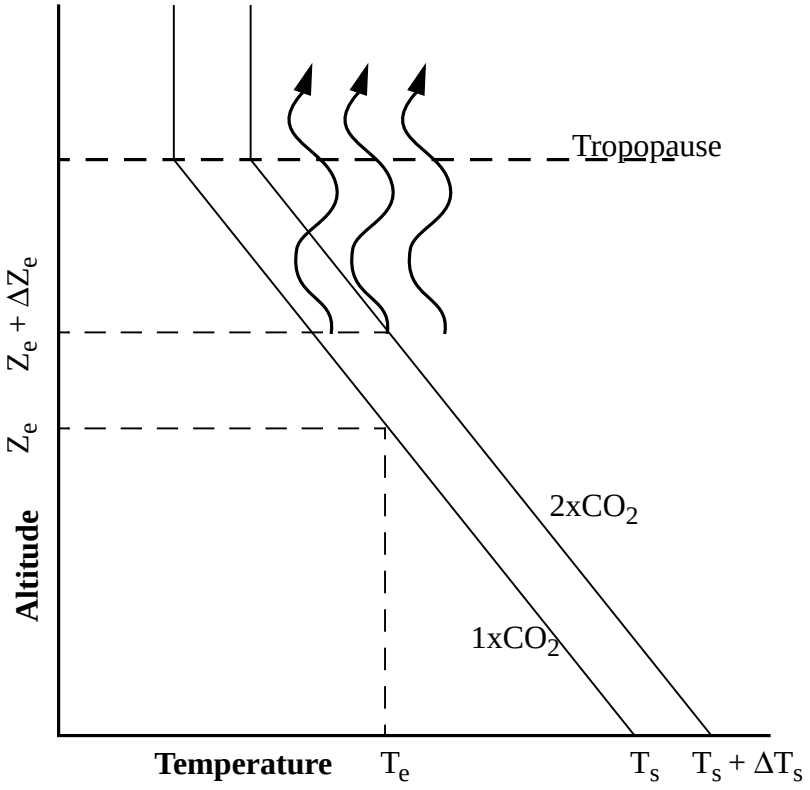

Figure 1: A schematic illustration of the change in emission level (Z_e) associated with an increase in surface temperature (T_s) due to a doubling of CO_2 assuming a fixed atmospheric lapse rate. Note that the effective emission temperature (T_e) remains unchanged.

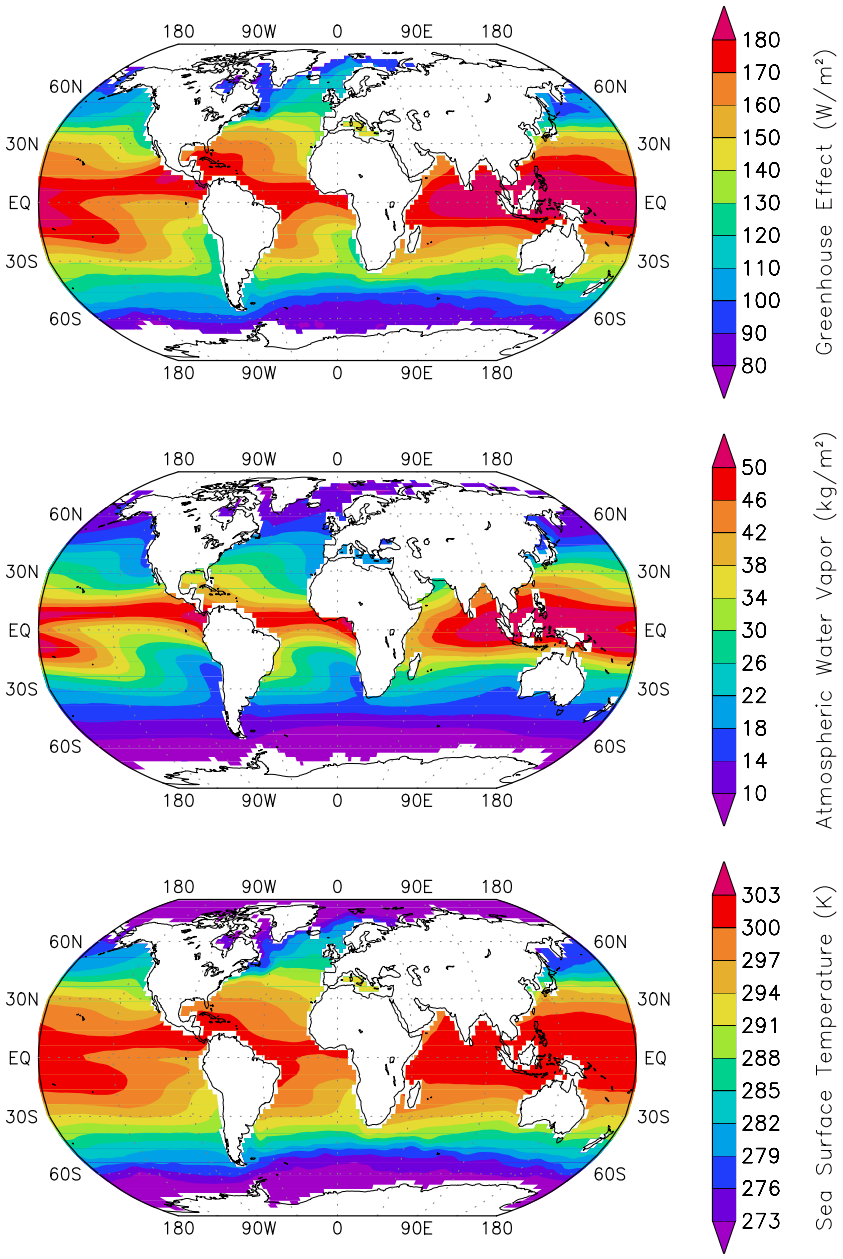

Figure 2: The annual-mean observed distribution of the clear-sky greenhouse effect G_{clear} (top), vertically-integrated water vapor concentration (middle), and sea surface temperature (bottom). Data are missing over land and ice-covered oceans due to uncertainties in their surface emission.

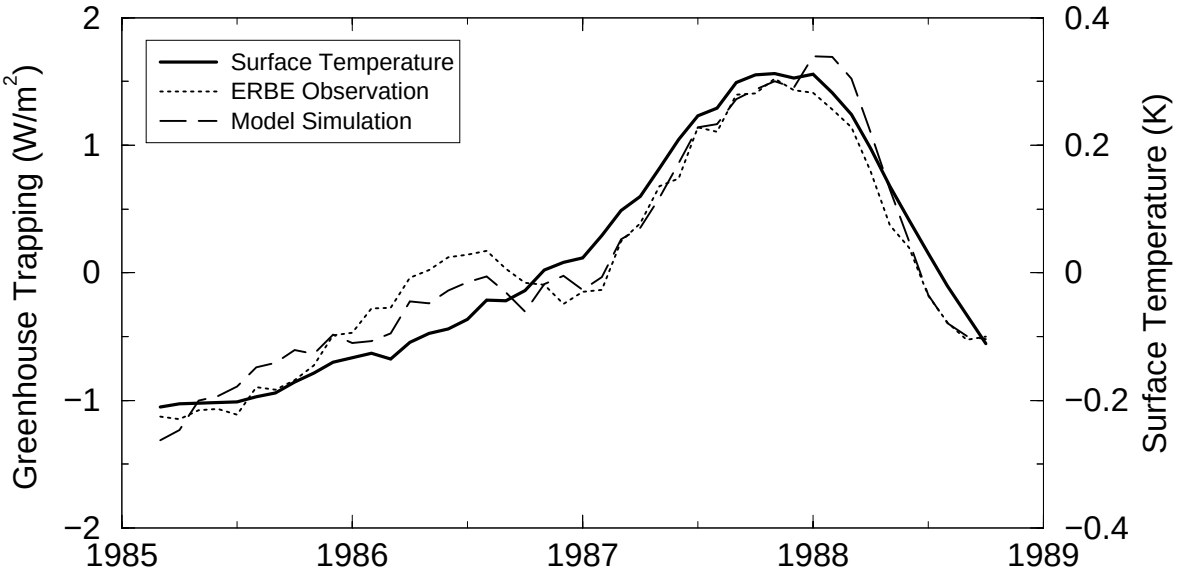

Figure 3: A time series of the tropical-mean interannual anomalies in clear-sky greenhouse trapping (G_{clear}) for 1985-1988 from ERBE observations (dashed line) and GFDL model simulations (dotted line). For reference, the tropical-mean anomalies in sea surface temperature are also shown (thick line).

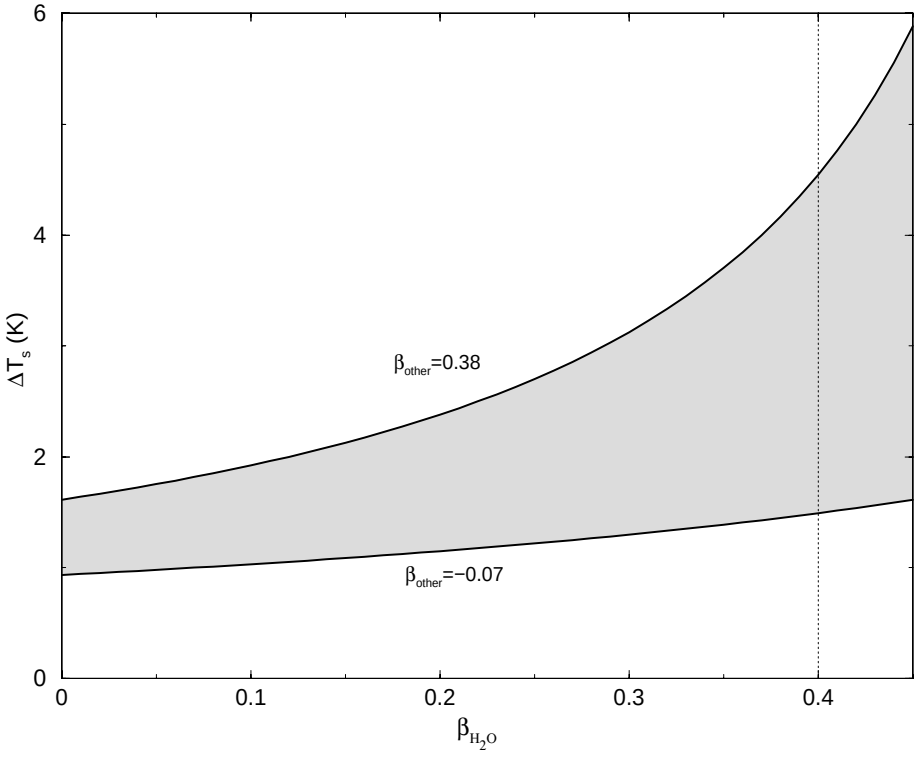

Figure 4: The change in surface temperature (ΔT_s) for doubled CO_2 as a function of the water vapor feedback parameter (β_{H2O}). Results are shown for two different scenarios of other temperature dependent feedbacks (β_{other}) that encompass the current range of predictions in ΔT_s=1.5-4.5 K when β_{H2O}=0.4.

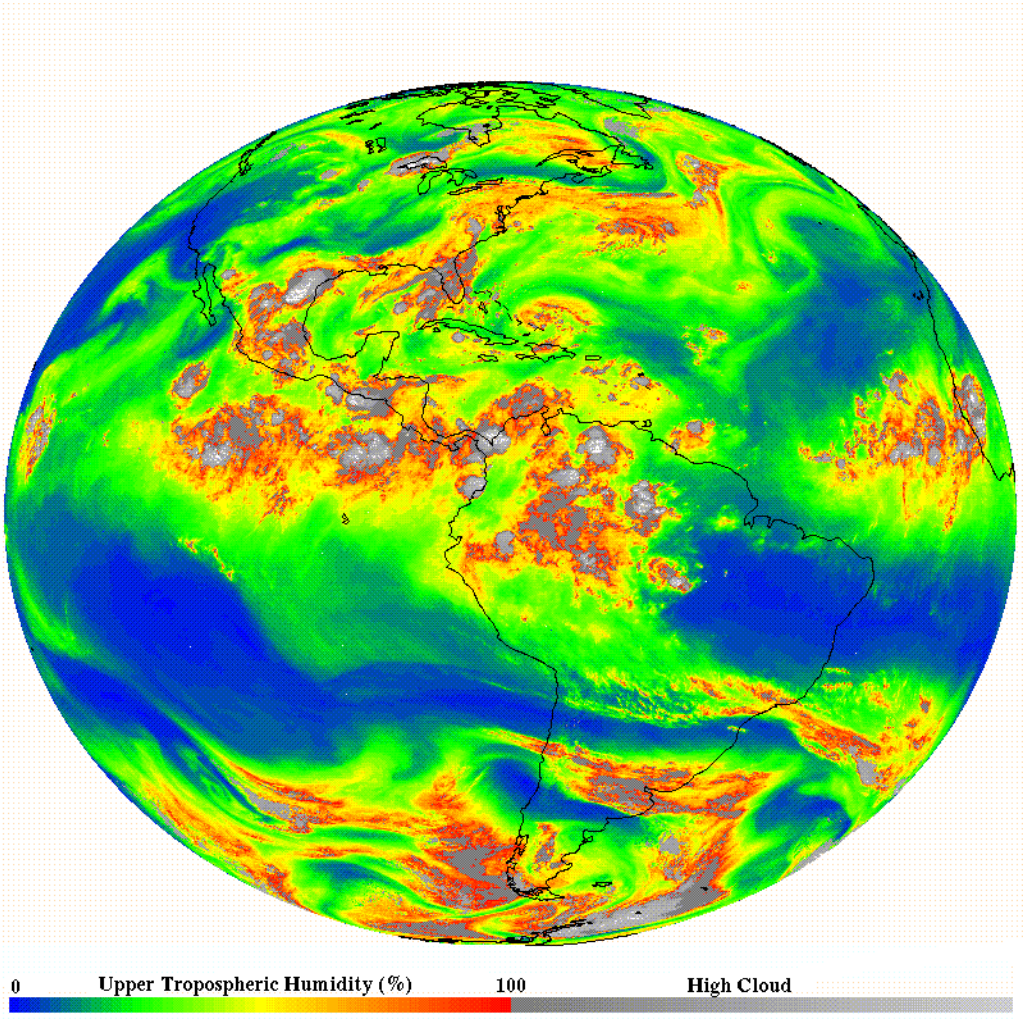

Figure 5: The upper tropospheric relative humidity (color) and cloud cover (grey) as observed from the Geostationary Operational Environmental Satellite (GOES-8) on April 27, 1999.

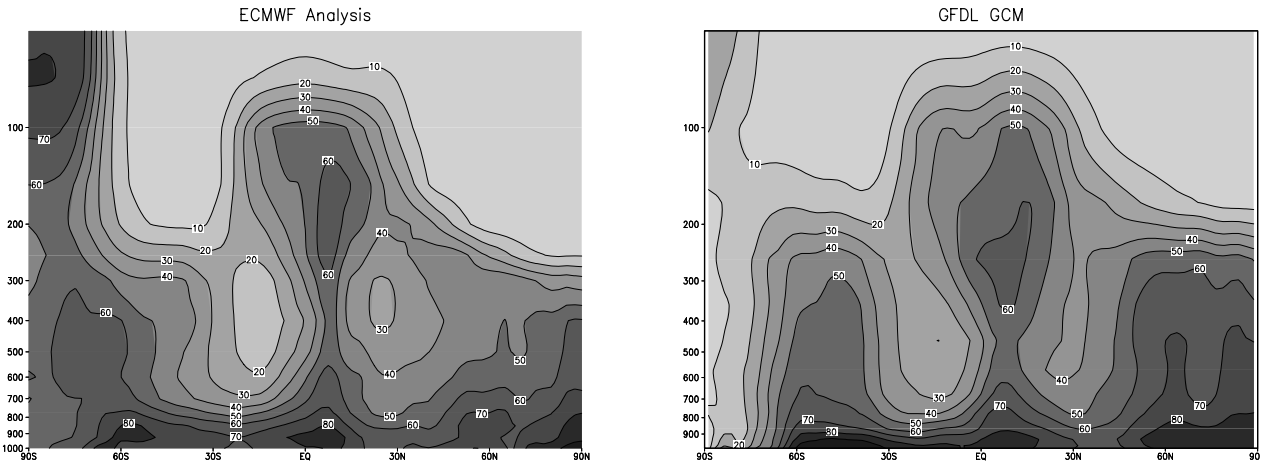

Figure 6: Height-latitude cross sections of the zonal-mean relative humidity for the month of July 1987 as produced by the European Centre for Medium-range Weather Forecasts (ECMWF) analysis system (left) and predicted by the GFDL General Circulation Model (GCM) (right).

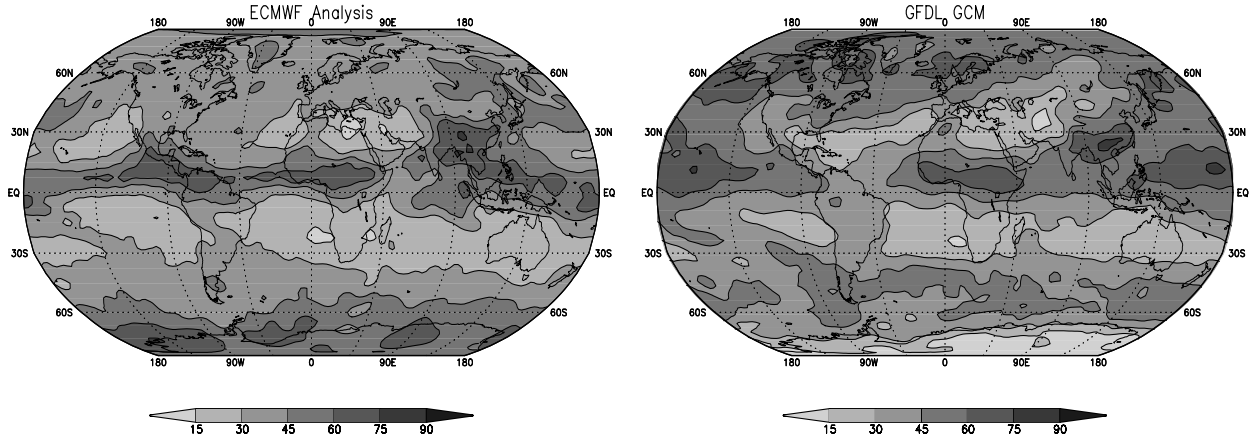

Figure 7: The geographic distribution of relative humidity, vertically-averaged over the free troposphere for July 1987 from the ECMWF analyses (left) and the GFDL GCM (right).

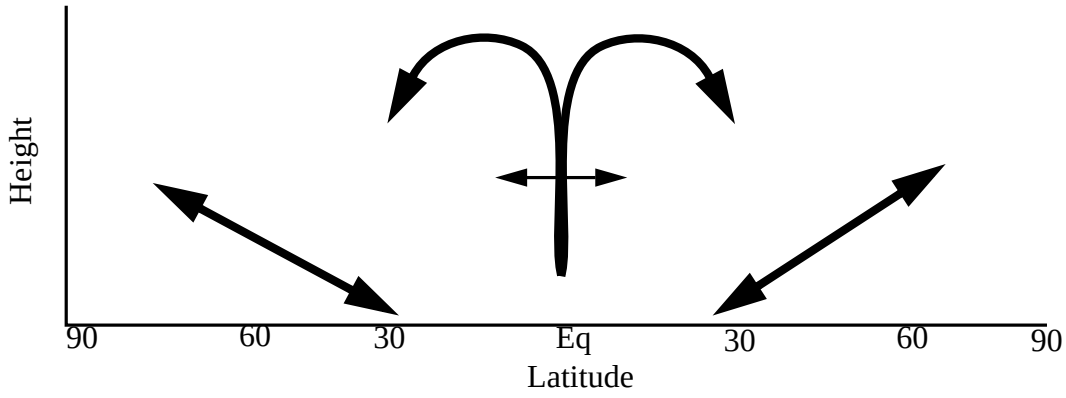

Figure 8: A height-latitude schematic of the large-scale atmospheric trajectories involved in the transport and mixing of moisture within the troposphere.

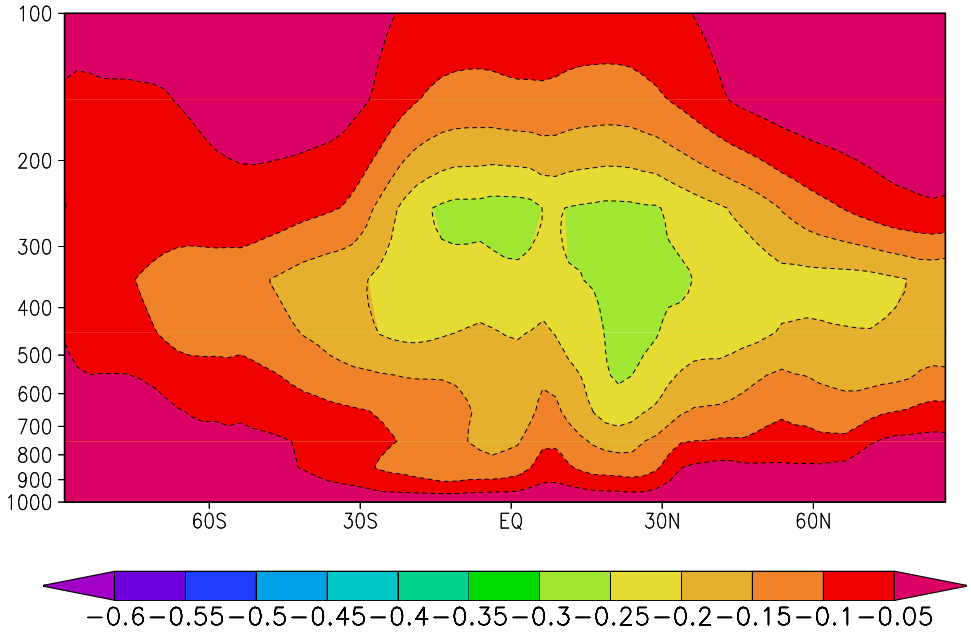

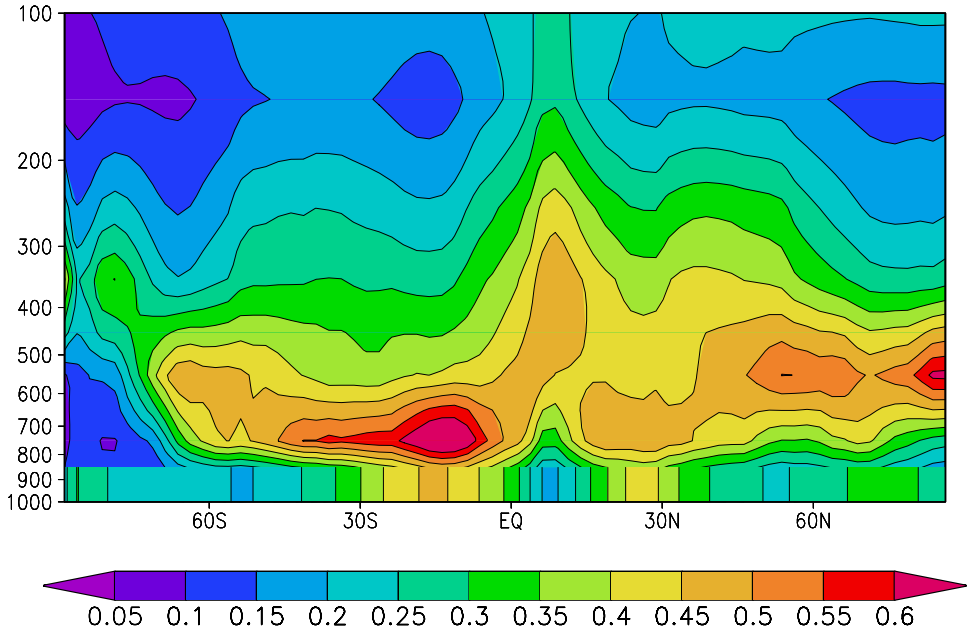

Figure 9: Height-latitude cross-sections of the sensitivity of the outgoing longwave radiation to perturbations in water vapor Q_e (top) and temperature Q_T (bottom) in 100 hPa thick layers. The results are expressed in units of $Wm^{-2}K^{-1}$.

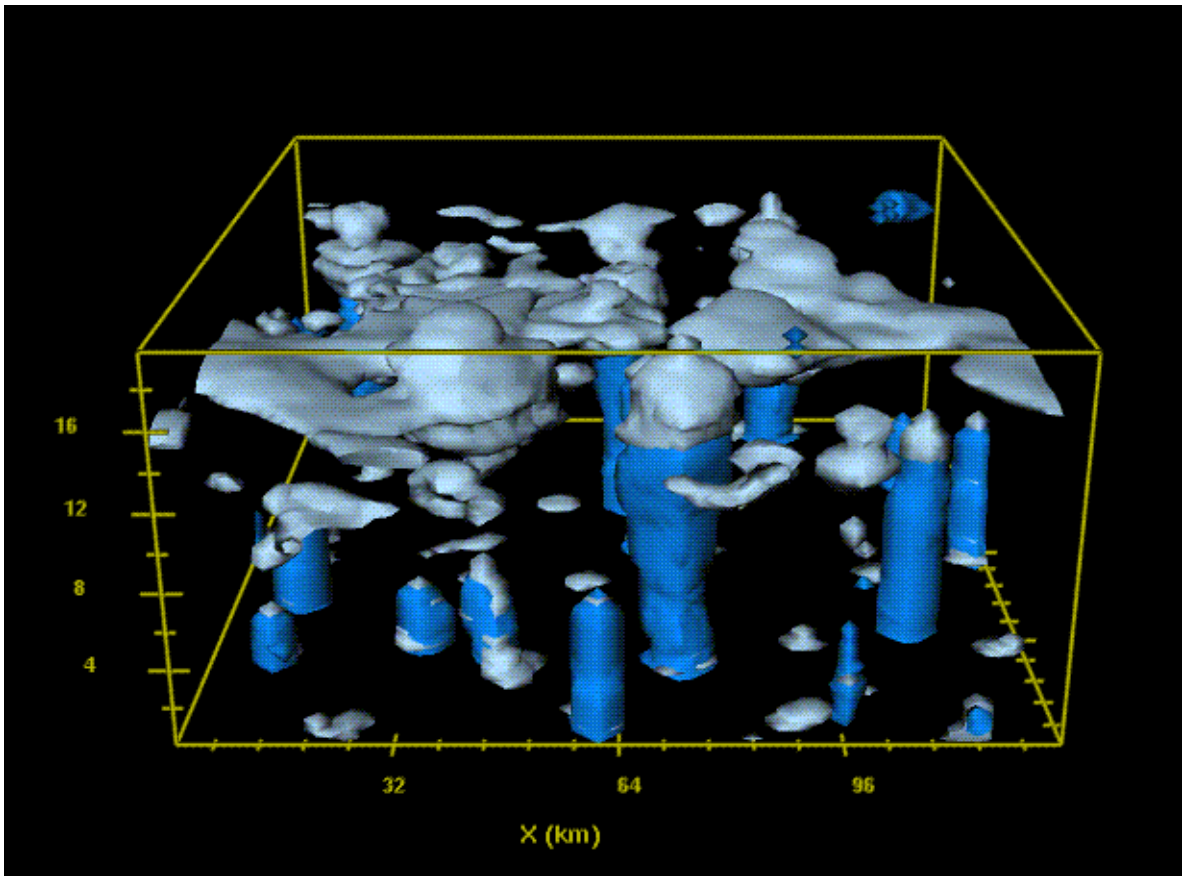

Figure 10: Distribution of cloud water (light blue) and precipitation (dark blue) simulated by the GFDL resolved cloud model. Note the difference in scale between the regions of active convection with respect to a typical GCM grid box (yellow box).